Title

Improved in vivo imaging of human blood circulation in the chorioretinal complex using phase variance method with new phase stabilized 1 μm swept-source optical coherence tomography (pv-SSOCT)

ISBN

9780819498434

Authors

Poddar, Raju
Kim, Dae Yu
Werner, John S
et al.

Publication Date

2014-02-28

DOI

10.1117/12.2040186

Peer reviewed

Improved *in vivo* imaging of human blood circulation in the chorioretinal complex using phase variance method with new phase stabilized 1 µm swept-source optical coherence tomography (pv-SSOCT)

Raju Poddar[*a], Dae Yu Kim[b], John S. Werner[a] and Robert J. Zawadzki[a,c]

[a]Vision Science and Advanced Retinal Imaging Laboratory (VSRI), Department of Ophthalmology & Vision Science, University of California Davis, Sacramento, CA95817, USA

[b]Biological Imaging Center, California Institute of Technology, Pasadena, CA 91125, USA

[c]UC Davis EyePod, Department of Cell Biology and Human Anatomy, University of California Davis, Davis, CA 95616, USA

ABSTRACTS

We demonstrate the feasibility of our newly developed phase stabilized high-speed (100 kHz A-scans/s) 1 µm swept-source optical coherence tomography (SSOCT) system with the phase-variance based motion contrast method for visualization of human chorioretinal complex microcirculation. Compared to our previously reported spectral domain (spectrometer based) phase-variance (pv)-SDOCT system it has advantages of higher sensitivity, reduced fringe wash-out for high blood flow speeds and deeper penetration in choroid. High phase stability SSOCT imaging was achieved by using a computationally efficient phase stabilization approach. This process does not require additional calibration hardware and complex numerical procedures. Our phase stabilization method is simple and can be employed in a variety of SS-OCT systems. Examples of vasculature in the chorioretinal complex imaged by pv-SSOCT is presented and compared to retinal images of the same volunteers acquired with fluorescein angiography (FA) and indocyanine green angiography (ICGA).

Keywords: Optical coherence tomography; Retinal blood flow; Ophthalmic optics and devices; Ophthalmology; Medical and biological imaging; Medical optics instrumentation.

1. INTRODUCTION

Numerous ophthalmic diseases, myopia, central serous chorioretinopathy (CSC), and age-related macular degeneration (AMD), are found to be linked to changes in choroid [1-2]. Most of the current clinical OCT technology, mainly SD-OCT, is operating in the 800-950 nm spectral band. This technology permits measurements of retinal vessels, but the ability to examine choroid is limited. This is mainly because the 800-nm-band probing beam is strongly scattered and absorbed by both the melanin in retinal pigment epithelium (RPE) and the choroid, and thus, penetration into the deep choroid is limited. It has been demonstrated that in order to obtain higher penetration into the choroid, one can use the OCT in 1-1.1µm spectral band [3]. Despite increased absorption by water for wavelengths above 950nm the low absorption of melanin at a wavelength of around 1.05 µm and presence of absorption minimum in the same range enables higher penetration into the choroid. Several groups have demonstrated retinal SD-OCT at 1-µm [4-5], but it performance is limited by strong fringe washout due to the high blood flow in choroid; short depth range and rapid sensitivity drop off. Thanks to advances in laser swept sources, swept-source (SS) OCT is now a good alternative for 1-µm range OCT imaging because of its advantages over SD-OCT, including robustness to motion [6], a long measurement range in depth due to short instantaneous line-width [7], k-linear sampling, compactness, and high imaging speed [8]. With current commercially available sources imaging the retina at 100 kHz compared to ~25 kHz in most commercial systems can be achieved in clinical instruments: for example DRIOCT-1, TOPCON swept source OCT [9].

*rpoddar@ucdavis.edu; phone 1 916-734-4541; Fax: 1 916-734-4543

Ophthalmic Technologies XXIV, edited by Fabrice Manns, Per G. Söderberg, Arthur Ho, Proc. of SPIE
Vol. 8930, 89300X · © 2014 SPIE · CCC code: 1605-7422/14/$18 · doi: 10.1117/12.2040186

Importantly, progress in phase stabilization schemes [10-13] and lack of fringe washout artifacts permit reliable mapping of fast flows.

There are several methods of increasing the contrast of vessels using the Doppler effect, such as Doppler standard deviation imaging [14], optical coherence angiography (OCA)[15] phase-variance OCT [16], and joint spectral and time domain OCT [17]. Pv-OCT [16], the methods implemented in our laboratory to extract flow contrast from SS-OCT images, can be used to visualize volumetric microvasculature independent of vessel orientation.

Standard SS-OCT suffers from jitter in synchronization between the wavelength sweep and data acquisition timing; this jitter causes small random spectral shifts among interference spectra and results in low phase stability. This low phase stability is a critical problem for phase-sensitive OCT modalities including phase-variance OCT. The problem was partially resolved by utilizing a stationary mirror or a glass plate in the sample arm [10]. It required however additional hardware in the sample arm, and thus, it made the system more complicated and limited the depth measurement range. Another approach to stabilize the phase is by using a separate Mach-Zehnder interferometer from an OCT interferometer [11] and numerical phase stabilization OCA [12]. Recently, one phase stabilization method was reported using a Fiber Bragg Grating (FBG) at one of the detection arms [18]. This system demonstrated good phase stability without sacrificing depth imaging range, but it still required additional hardware and computational complexity.

We have described recently [19] a new, simple and robust method for phase stabilization using A-line trigger from a high stabilized Fiber Bragg Grating (FBG) and numerical phase stabilization, without any major additional calibration hardware changes. Here, we describe modifications of this system allowing mapping of blood circulation in different layers of the chorioretinal complex of a normal human eye *in-vivo*.

2. MATERIALS AND METHODS

2.1. Phase-variance SSOCT system

A schematic diagram of our 1μm SSOCT system used for anterior segment imaging was already reported previously [19]. Here, we briefly describe changes to our SSOCT system (Fig.1) allowing posterior segment imaging. The light source was an external cavity tunable laser (ECTL), swept-source laser (Axsun Technologies), with a central wavelength of 1060nm, sweep bandwidth of 110 nm, repetition rate of 100 kHz, 46% duty cycle and average output power of ~23 mW. A spectrally balanced interferometer configuration was used with three 50/50 fiber couplers (AC Photonics), and a balanced Mach-Zehnder fiber interferometer. The sample port was attached to a probe unit, which comprises a fiber collimator lens (12.38 mm, focal length, TC12APC-1064, Thorlabs, Inc.), two one axis galvano scanners (Cambridge Technology), and two achromatic doublets of focal length 50 mm and 30 mm (AC254-030-C-ML, Thorlabs, Inc.). The reference port of the fiber coupler was attached to a reference arm unit comprising a collimator lens, an achromatic doublet lens, dispersion compensating block and a static silver-coated mirror.

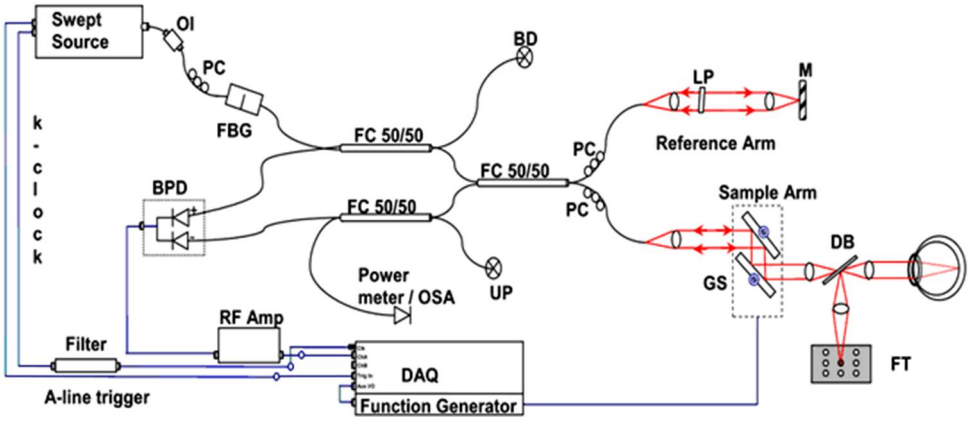

Figure 1. Schematic diagram of pv-SSOCT system. Swept source laser 1060 nm Axsun ECTL. FBG: Fiber Bragg Grating, FC: Fiber Coupler, GS: galvano scanning mirrors, M: mirror, BPD: balanced photo diode receiver (DC to 350 MHz, PDB130C, Thorlabs), PC: polarization controller, LP: linear polarizer, RF Amp: Radio Frequency amplifier (Minicircuits ZFL-1000+), DB: Dichroic

Beamsplitter, FT: Fixation Target, BD: Beam dump, UP: unused port, OSA: optical spectrum analyzer, DAQ: digitizer (ATS9350, AlazarTech, 12-bit resolution and sampling rate of 500 MS/s), Function generator (NI PCI-6363, National Instruments, TX).

2.2. Image acquisition and data processing for pv-SSOCT

The galvanometric scanners steer the probe beam was controlled by Digital I/O board (PCI-6363, National Instruments, TX). The probing beam power at the sample was set as 1.85 mW, which is lower than the ANSI for safe light exposure (ANSI Z136.1 standard)]. The reflected beams from both arms of interferometer were combined at the couplers and detected by a balanced photo-detector with a bandwidth of DC to 350 MHz (PDB130C, Thorlabs Inc.) followed by an RF amplifier and high-pass filter (Minicircuits ZFL-1000+). The OCT interference signal was digitized by a data acquisition (DAQ) board at 12-bit digital resolution at sampling rate defined by external trigger provided by Axsun Swept Source k-clock (ATS9350, AlazarTech, QC, Canada).

Here, a novel and robust method for phase stabilization [19] arises due to A-line trigger fluctuations. A fixed wavelength reference signal generated by a fiber Bragg grating (FBG, OE Land, Quebec, Canada, λ_0 = 988.9 nm, reflectivity = 99.91%, $\Delta\lambda$ = 0.4 nm) inserted in transmission mode between the source and OCT interferometer (Fig. 1) was used to align in post-processing each A-line start trigger time. This has several advantages from other existing methods. The necessary shifts in the acquired SS-OCT signal can be calculated based on the first falling slope of the signal around the FBG signal. This phase-stabilization method was adopted before phase variance calculation. The accuracy of phase-stabilization is discussed in section 2.3. These results in measurement phase-shifts at a noise-level down to the theoretical limit (see section 2.3.1), to completely remove fixed-pattern noise and to obtain artifact free phase variance contrast images.

Synchronization between data acquisition and the galvanometric scanner is achieved in the build sweep trigger signal of the laser source, which is utilized for triggering the data acquisition of the DAQ for a single sweep and utilized as an update clock for the waveform generation for galvanometric scanning. Subject's gaze is stabilized using a custom-built fixation target reflected through a dichroic beamsplitter (FF775-Di01, Semrock). The fixation target is a mini LCD screen (MIMO, USA) and controlled by computer to switch fixation light position. Acquisition with LabVIEW software (National Instruments) required 1 to 2 seconds depending on scanning pattern settings. The raw data are stored in the workstation (HP xw8600, 3.2-GHz dual processors). Data sampling was performed using an optically generated clock signal with equi-spacing in wavenumber, namely, a k-clock from laser source. Owing to this k-linear sampling, no rescaling process is required before Fourier transform of the spectral data.

Pv-SSOCT data sets were obtained in the Vision Science and Advanced Retinal Imaging laboratory (VSRI) at the University of California Davis Medical Center on a 62-year-old healthy subject with normal ocular media. Written informed consent was obtained prior to imaging approved by the institutional review board (IRB). The subject's head position was fixed during acquisition using a custom bite-bar and forehead rest. There was no need for pupil dilation. Scanning areas of the retina were 3x3 mm^2 and 1.5x1.5 mm^2. A BM-scanning mode (multiple B-scans at the same position) was used to acquire the phase-change measurements required to calculate the phase-variance contrast. For the 1.5x1.5 mm^2 scanning pattern, 4.2 μm spacing between both consecutive A-scans and BM-scans was used. Due to the spatial oversampling between consecutive BM-scans, phase changes from within two adjacent BM-scans were used for the variance calculations. Three B-scans were acquired within each BM-scan, producing two phase change measurements for each BM-scan. The A-line exposure time was 4.2 μs and the spectral data were saved in a binary file format for post-processing in LabVIEW software. All images shown in this manuscript were acquired *in vivo* at 100,000 axial scans (A-scan) rate per second.

Acquired OCT data (already linear in k-space) was first aligned based on the reference FBG signal. Fixed-pattern noise was removed by subtracting the B-scan average spectrum from each individual A-line spectrum. The resultant spectra were windowed to minimize side-lobes of the coherence function by apodization with a flat top Gaussian window [11]. Optical chromatic dispersion was numerically compensated by automatic dispersion compensation based on an entropy minimization method [15]. Finally a complex SSOCT signal with intensity and phase information was obtained after Fourier-transformation of the processed and zero padded (to 4096 points) data.

Fall-off profiles from the 1060 nm system were measured using standard procedures [11] and reported in our previous published work [19]. Each B-scan consisted of 440 A-scans acquired over a 1.5 mm lateral scanning range. The dynamic range of the intensity image was 35 dB and the phase values varied from $-\pi$ to $+\pi$. The basic concept of this method was

already discussed in our previous work [16]. The acquired preprocessed OCT data sets were post-processed by software developed at the Biological Imaging Center at the California Institute of Technology to extract phase-variance signals. The cross-correlation function between consecutive intensity images aligns each B-scan from a BM-scan in an axial direction. Phase unwrapping on phase difference values, bulk motion removal and histogram-based thresholding processing were implemented to remove phase shifts caused by eye motion. To visualize two- and three-dimensional vasculature networks in chorioretinal complex, the three dimensional phase-variance data sets were manually segmented from the layer as per prior literature. The en face projection view of the segmented data produced two-dimensional vascular perfusion maps which were similar to the ones obtained with fundus FA. The FA images (1280x1024 pixels) shown in this paper were acquired with a Topcon (TRC-50IX) fundus camera. Pseudo-color (red-green-blue (RGB) coding of the processed volumetric data sets was used to better visualize three-dimensional vessel networks and its projection view created two-dimensional color vasculature imaging linearly scaled by axial depth location of the vessels.

2.3. Phase-stability analysis

The accuracy of phase-variance measurements and the removal of fixed-pattern noise both depend on the phase-stability performance of the SSOCT system. Phase-stability can be measured by analyzing the phase-difference between successive A-lines as measured on a stationary mirror [11]. A mean phase-noise value of 40 mrad was measured at a depth of 1.5 mm for SNRs of 50 dB. This is comparable to previously published results for SSOCT systems phase-noise, e.g., Hendargo et al. 18 mrad for 53 dB SNR, [13] and Baumann et al. (97 mrad at 100 kHz and 47 mrad at 200 kHz for a 35 dB SNR) [10].

2.4. Imaging performance:

2.4.1 Fixed-pattern noise and Phase-noise artifact removal in flow imaging

The effect of applying the phase-stabilization method before OCT and pv-OCT processing is shown on B-scans acquired at 6° temporal retina (Fig 2). The intensity images are shown in Fig. 2 (A, D). Each intensity B-scan image covers retinal lateral area of 1.5 mm consisting of 440 A-lines, a displayed depth of 1.5 mm, and a dynamic range of 35.0 dB. The corresponding phase variance images (Figs. 2 B, E) have the same dimensions. A 2D median filter (3x10 pixels) was used for noise reduction. In Fig. 2B the phase variance image is shown when the phase-stabilization method was not used, which resulted in horizontal (yellow arrow) as well as vertical (green arrow) phase-artifact lines throughout the imaged tissue, obscuring a clear view on the detected blood-flow. These artifacts are however totally absent when the phase-stabilization method was used as shown in Fig. 2E. The same effect can be also observed on en face projection images in Fig 2 (C, F).

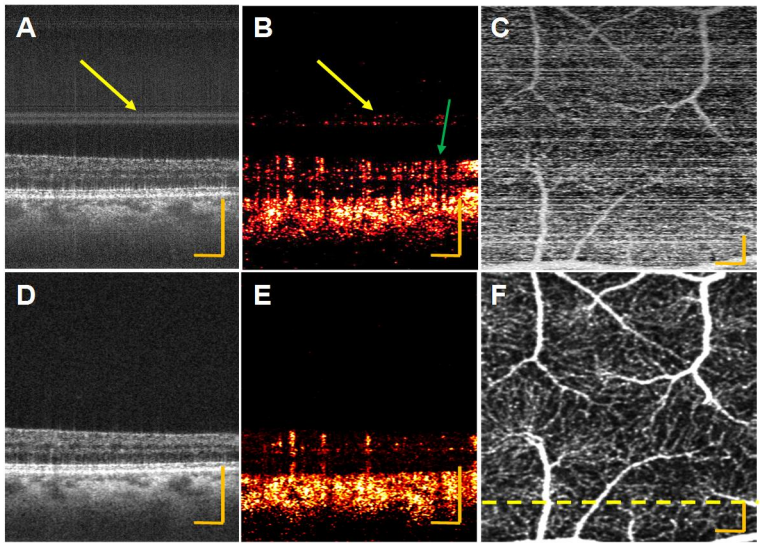

Figure 2. Top and bottom panels show images before and after phase stabilization, respectively**.** Average intensity image of three B- scans (A,D) Phase-variance processed image using phase data from the same three B-scans (B,E), En face projection of retinal vasculature(C,F); yellow dashed line in panel F shows the location of B-scan. Vertical phase-artifact lines (Yellow arrow) and horizontal lines (green arrow) can be seen throughout the images processed without phase stabilization (A, B). Scale bar: 350 μm.

3. RESULTS AND DISCUSSION

3. 1. Three-dimensional imaging of chorio-retinal vascular network

BM-scans data were acquired over a 1.5x1.5 mm^2 area of the human retina with more densely sampled A-scans (sampling spacing was 4 μm between A-scans) for clear visualization of micro-circulation. The scanning beam was focused on RPE to improve visualization of the outer retinal layers and the blood supply in the choroid and choriocapillaris. An average intensity image composed of three successive B-scans from a single BM-scan is shown in Fig. 3 (a). Fig. 3 (b) shows the image post-processed with the phase-variance method from these data. The combined image with averaged intensity and phase variance, red color-coded is shown in Fig.3 (c). There was no significant eye motion during BM-scan acquisition due to short acquisition times of each B-scan (approximately 3.5 ms). The composite image validates that pvOCT identifies most of perfusion structures compared with the average intensity imaging where vessels can be classified based on their increased intensity. There is a so-called shadow artifact that generates residual phase-variance values below vessels. This result in non-zero phase-variance values calculated in retinal layers where no perfusion should be observed including in the retina pigmented epithelium and deep choroidal layers. More phase variance signal in deeper choroid was observed compared to our previously reported SDOCT based phase variance [20]. This was possible due to higher OCT sensitivity offered by a balanced detection scheme in SS-OCT, and by use of a 1060 nm central wavelength to increase penetration depth of our imaging light and improve contrast below the RPE. Additional benefits include a long measurement range in depth due to short instantaneous line-width of the source, permitting OCT image intensity at distances further away from the zero path-length difference than possible with spectrometer-based OCT. Thus, even with modest axial head motion of the patient from the forehead rest during automatic acquisition of several microvolumes, image quality was not impaired by relative changes of the location of the imaged structures to the reference arm position.

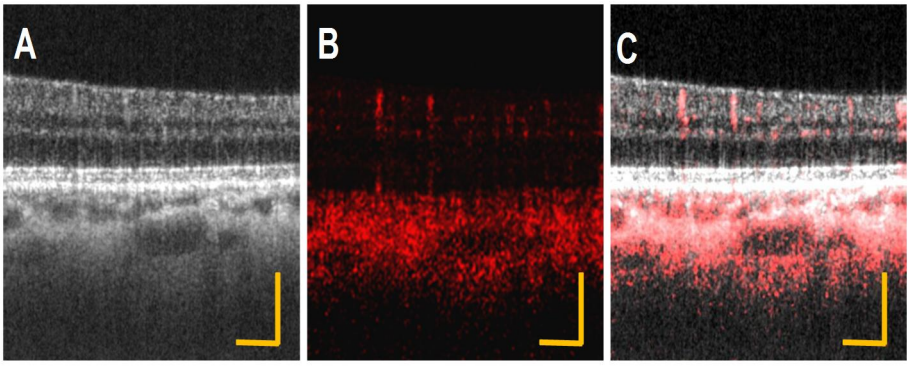

Figure 3. Human retinal images of phase-variance OCT data processing over 1.5 mm. (a) Average intensity imaging of three B-scans from a single BM-scan. (b) Phase-variance image. (c) Combined image of average intensity (a) and red color-coded phase-variance imaging (b). The imaging acquisition time of a single BM-scan containing three B-scans is approximately 12 ms. Scale bar: 300 μm.

The left eye of the subject was imaged with FA and pv-SSOCT. Images illustrated in Fig. 4 were acquired over 1.5x1.5 mm^2 of the human foveal region. We compared maximum projection view of pvOCT in Fig. 4B to the fundus FA in Fig. 4A, acquired at the same location. Figure 4B shows dense micro-capillary networks around foveal evascular zone, not distinctly recognizable in the zoomed fundus FA image. The size of the smallest resolvable capillary in this acquisition scheme was 10~12 μm. Fig. 4C shows a depth color-coded projection view. The pseudo-color (RGB) map codes the

linearly-scaled axial location of the vessels.

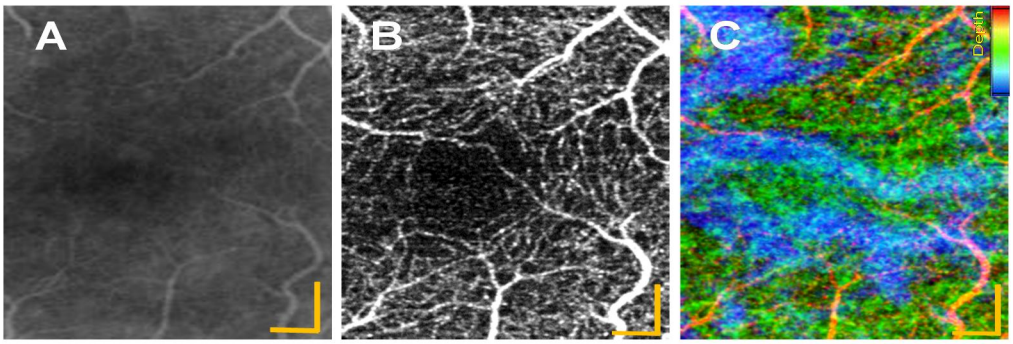

Figure 4. *In vivo* human retinal vasculature images (1.5x1.5 mm^2) from a normal subject. (a) Fluorescein angiography. (b) A projection image of phase-variance OCT retinal layers. The imaging acquisition time was 3.6 seconds. Scale bar: 500μm.

Depth-resolved pv-SSOCT projections and corresponding FA and ICGA images are shown in Fig.5. The retinal capillary network (within the nerve fiber layer to outer nuclear layer), is coded as red (Fig 5C). Choriocapillaris marked at different depths (6 μm below Bruch's membrane coded as gray**)** were generated from the OCT phase variance volume (5D).). Here, shadow artifacts from large retinal vessels (marked with yellow arrows) are observed on choriocapilaries layer. They are not part of choroidal vasculature. Fig 5E is showing an en face angiogram extracted from the same volumetric data sets from 26 μm to 34 μm below Bruch's membrane where feeding arterioles and draining venules in the Sattler's layer are clearly visualized. The Haller's layer consists of larger feeder vessels, located from 61 μm to 90 μm below Bruch's membrane, shown in Fig 5F. The ICGA (5H) and corresponding pv-SSOCT total choriodal projection in gray scale (5H) is presented. The pseudo-color (RGB) coded depth projection is also presented in Fig 5I. There is excellent correspondence of structural features between the OCT angiograms and the electron micrograph corrosion casts reported by Olver et al. [21]. Deep penetration from SSpvOCT is capable of *in vivo* visualization of the chorioretinal complex.

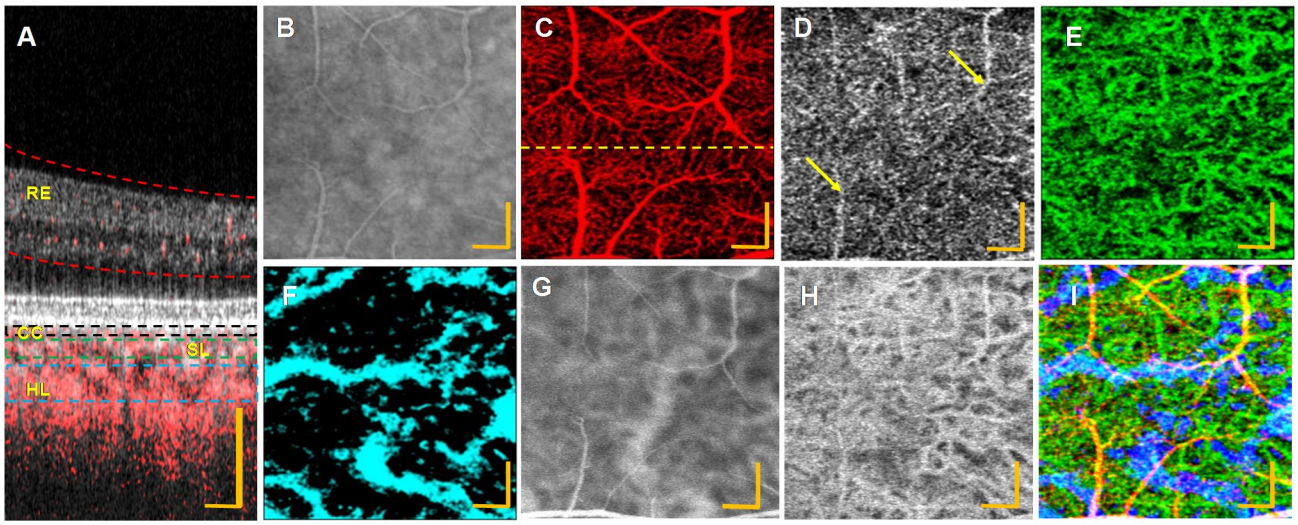

Figure 5. SSpvOCT volumetric scan over 1.5x1.5 mm^2 at 6° temporal retina. (A) Composite B-scan image showing flow signal in different retinal and choroidal layers overlaid over intensity image, and (B) corresponding FA image, Segmented depths for en-face projection images are: (C) retinal layers, (D) 6 μm below Bruch's membrane for choriocapillaris (E) 26 μm to 34 μm below Bruch's membrane for Sattler's layer; (F) 61 μm to 90 μm below Bruch's membrane for Haller's layer; (G) corresponding ICGA image, (H) total enface projection of choriodal layer only in gray scale, and, (I) depth color-coded enface projection. Yellow arrows in (D) show the shadow artifact from big retinal vessels projected on choriocapillaris layer. Scale bars, 300 μm. Morphological features here resemble histological images by corrosion vascular casts and scanning electron microscopy [21].

4. CONCLUSION

In this paper we demonstrate feasibility of a phase variance based high-speed 1 μm swept source optical coherence tomography system for *in vivo*, noncontact and noninvasive two-dimensional visualization of the vasculature of chorioretinal complex. The pv-SSOCT produces details of vascular capillary networks comparable to fundus FA without the need for exogenous contrast agents. Densely scanning a small field of view, 1.5x1.5 mm^2, generates the microcapillary perfusion map and color-coded depth information of the microvasculature. The pv-SSOCT angiography is capable of generating integrated imaging of both retinal and choroidal structures and vasculature. Our data suggest that pv-SSOCT has potential in the early diagnosis of retinal vascular diseases including age-related macular degeneration, better understanding of pathogenesis, and study of treatment response and efficiency of pharmaceutical agents.

5. ACKNOWLEDGMENTS

We gratefully acknowledge the contributions of VSRI UC Davis lab members and the Biological Imaging Center at the California Institute of Technology for supporting the phase-variance post-processing software. This research was supported by the National Eye Institute (EY 014743) and Research to Prevent Blindness (RPB).

REFERENCES

[1] Imamura, Y., Fujiwara, T., Margolis, R. and Spaide, R. F., "Enhanced depth imaging optical coherence tomography of the choroid in central serous chorioretinopathy," Retina 29, 1469–1473 (2009).
[2] Chakravarthy, U., Evans, J., and Rosenfeld, P. J., "Age related macular degeneration," Br. Med. J. 340 (2010).
[3] Unterhuber, A., Povaˇzay, B., Hermann, B., Sattmann, H., Chavez-Pirson, A. and Drexler, W., "*In vivo* retinal optical coherence tomography at 1040 nm enhanced penetration into the choroid," Opt. Express 13, 3252–3258 (2005),
[4] Yasuno, Y., Hong, Y., Makita, S., Yamanari, M., Akiba, M., Miura, M., and Yatagai, T., "*In vivo* high-contrast imaging of deep posterior eye by 1-um swept source optical coherence tomography and scattering optical coherence angiography," Opt. Express 15, 6121–6139 (2007).
[5] Srinivasan, V. J., Adler, D. C., Chen, Y., Gorczynska, I., Huber, R., Duker, J. S., Schuman, J. S. and Fujimoto, J. G., "Ultrahigh-speed optical coherence tomography for three-dimensional and en face imaging of the retina and optic nerve head," Invest. Ophthalmol. Vis. Sci. 49, 5103–5110 (2008).
[6] Yun, S. H., Tearney, G., de Boer, J. and Bouma, B., "Motion artifacts in optical coherence tomography with frequency-domain ranging," Opt. Express 12, 2977–2998 (2004).
[7] Potsaid, B., Baumann, B., Huang, D., Barry, S., Cable, A. E., Schuman, J. S., Duker, J. S. and Fujimoto, J. G., "Ultrahigh speed 1050nm swept source/fourier domain OCT retinal and anterior segment imaging at 100,000 to 400,000 axial scans per second," Opt. Express 18, 20029–20048 (2010).
[8] Klein, T., Wieser, W., Eigenwillig, C. M., Biedermann, B. R. and Huber, R., "Megahertz OCT for ultrawide-field retinal imaging with a 1050nm fourier domain mode-locked laser," Opt. Express 19, 3044–3062 (2011).
[9] http://www.topcon-medical.eu/eu/products/177-dri-oct-1-swept-source-oct.html, 10 Dec, 2013.
[10] Baumann, B., Potsaid, B., Kraus, M. F., Liu, J. J., Huang, D., Hornegger, J., Cable, A. E., Duker, J. S. and Fujimoto, J. G., "Total retinal blood flow measurement with ultrahigh speed swept source/fourier domain OCT," Biomed. Opt. Express 2, 1539-1552 (2011).
[11] Braaf, B., Vermeer, K. A., Sicam, V. A. D., van Zeeburg, E., van Meurs, J. C. and de Boer, J. F., "Phase-stabilized optical frequency domain imaging at 1-μm for the measurement of blood flow in the human choroid," Opt. Express 19, 20886-20903 (2011).
[12] Hong, Y., Makita, S., Jaillon, F., Jin Ju, M., Eun Jung Min, Lee, B. H., Itoh, M., Miura, M. and Yasuno, Y., "High-penetration swept source Doppler optical coherence angiography by fully numerical phase stabilization", Biomedical Opt. Express, Vol. 20 (3), 2740- 2760, (2012).
[13] Hendargo, H.C., et al "Doppler velocity detection limitations in spectrometer-based versus swept-source optical coherence tomography", Biomedical Opt. Express,Vol. 2 (8),2175-2188, (2011).
[14] Zhao, Y., Chen, Z., Saxer, C., Shen, Q., Xiang, S., de Boer, J. F. and Nelson, J. S. "Doppler standard deviation imaging for clinical monitoring of *in vivo* human skin blood flow," Opt. Lett. 25, 1358–1360 (2000).
[15] Makita, S., Hong, Y., Yamanari, M., Yatagai, T. and Yasuno, Y., "Optical coherence angiography," Opt. Express 14, 7821–7840 (2006).

[16] Kim, D. Y., Fingler, J., Werner, J. S., Schwartz, D. M., Fraser, S. E. and Zawadzki, R. J., "*In vivo* volumetric imaging of human retinal circulation with phase-variance optical coherence tomography," Biomed. Opt. Express 2, 1504–1513 (2011).
[17] Szkulmowski, M., Szkulmowska, A., Bajraszewski, T., Kowalczyk, A. and Wojtkowski, M., "Flow velocity estimation using joint spectral and time domain optical coherence tomography," Opt. Express 16, 6008–6025 (2008)
[18] Choi, W. J. et al. "Phase-sensitive swept-source optical coherence tomography imaging of the human retina with a vertical cavity surface-emitting laser light source", Optics Letters, Vol. 38 (3), 338-340, (2013).
[19] Poddar, R., Cortes, D., Zawadzki, R. J., Mannis, M. J. and Werner, J. S., "Three-dimensional anterior segment imaging in patients with type 1 Boston Keratoprosthesis with switchable full depth range swept source optical coherence tomography"; Journal of Biomedical Optics 18(8), 086002 (2013).
[20] Kim, D. Y., Fingler, J., Zawadzki, R. J., Park, S. S., Morse, L. S., Schwartz, D. M., Fraser, S. E., and Werner, J. S., "Optical imaging of the chorioretinal vasculature in the living human eye," Proc Natl Acad Sci U S A, 110,14354–9 (2013).
[21] Olver, J. M. et al, "Functional anatomy of the choroidal circulation: Methyl methacrylate casting of human choroid. Eye", 4, 262–272 (1990).